JOURNAL OF THERMOPHYSICS AND HEAT TRANSFER
Vol. 22, No. 3, July–September 2008

Convective Heat Transfer from a NACA Airfoil at Varying Angles of Attack

X. Wang*
University of Manitoba, Winnipeg, Manitoba R3T 5VC, Canada
G. F. Naterer†
University of Ontario Institute of Technology, Oshawa, Ontario L1H 7K4, Canada
and
E. Bibeau‡
University of Manitoba, Winnipeg, Manitoba R3T 5VC, Canada

DOI: 10.2514/1.34405

Airfoil icing in aircraft and wind turbine applications has an adverse impact on aerodynamic performance, controllability, and system efficiency. A detailed understanding of convective heat transfer from airfoils is critical in the development of effective de-icing methods. In this paper, experimental correlations of heat transfer at different angles of attack of a NACA 63-421 airfoil are developed. Various angles of attack between 0 to 25 deg are investigated at different Reynolds numbers. The experimental data are correlated with respect to the Nusselt and Reynolds numbers, through a modified Hilpert correlation with an angular dependence on angles of attack. Conduction within the airfoil is balanced against heat transfer by convection from the airfoil surface in steady-state conditions. Both average and spatial variations of the heat transfer coefficients are nondimensionalized, through modifications of a Hilpert correlation for cylinders in crossflow. It is shown that the functional form of the Hilpert equation can effectively correlate the measured data for the NACA airfoil over a range of Reynolds numbers and angles of attack.

Nomenclature

C_1	=	chord coefficient
c	=	chord length of airfoil, m
c_m	=	moment center, $c/4$
D_1, D_2	=	arc angle coefficients
$\bar{h}$	=	average heat convection coefficient, $\mathrm{W/m^2K}$
h_i	=	local heat convection coefficient, $\mathrm{W/m^2\,K}$
k	=	thermal conductivity, W/mK
$\overline{Nu}$	=	average Nusselt number
Nu_x	=	local Nusselt number
Pr	=	Prandtl number
Re_c	=	Reynolds number (reference length: chord)
Re_D	=	Reynolds number (reference length: diameter of a sphere)
Re_x	=	Reynolds number (reference length: position along a flat plate)
T_i	=	inner surface temperature of airfoil, °C
T_o	=	outer surface temperature of airfoil, °C
T_∞	=	freestream temperature, °C
α	=	angle of attack
δ	=	thickness of airfoil, m
μ	=	dynamic viscosity of air, kg/ms
ρ	=	density of air, $\mathrm{kg/m^3}$

Received 3 September 2007; revision received 16 December 2007; accepted for publication 17 December 2007.

*Ph.D. Candidate, Department of Mechanical and Manufacturing Engineering, 75 Chancellors Circle, Winnipeg.

†Professor of Mechanical Engineering and Canada Research Chair in Advanced Energy Systems, Faculty of Engineering and Applied Science, 2000 Simcoe Street North.

‡Assistant Professor and Manitoba Hydro/NSERC Alternative Energy Chair, Department of Mechanical and Manufacturing Engineering, 75A Chancellors Circle.

I. Introduction

FORCED convection heat transfer from standard geometrical configurations such as cylinders, plates, and spheres has been studied and reported extensively in past literature. For basic configurations such as a flat plate, analytical expressions can be developed for the Nusselt number, in terms of the Reynolds and Prandtl numbers. For other bluff bodies, empirical correlations based on experimental data are often required. A standard functional form for these correlations involves a product of Reynolds and Prandtl numbers, raised to exponents that depend on various physical factors, such as flow conditions and geometrical parameters [1]. Few studies of Nusselt number correlations have been performed for airfoils, particularly over different ranges of airfoil inclination. In this paper, experimental data are collected for airfoils into a new functional correlation that includes the dependence of Nusselt number on the angle of attack. These results can have valuable utility for airfoil de-icing predictions, during early stages of ice growth when the surface still resembles an airfoil shape.

Past studies by Van Fossen et al. [2] investigated heat transfer from a cylinder with four simulated ice shapes. Heat transfer correlations for a circular cylinder with different ice shapes and surface roughnesses were developed with the NASA Glenn Icing Research Tunnel, using heat flux gages, strip heaters, and hot wires. Henry et al. [3] measured heat transfer coefficients for an iced airfoil with a laser pulse method and infrared camera. Iced shapes were formed at −25°C and 1 $\mathrm{g/m^3}$ liquid water content. Heat transfer coefficients were presented at different velocities and ice shapes. Unlike this study by Henry et al. [3] (which did not fully correlate the data), this paper develops a Nusselt correlation for convective heat transfer from an airfoil surface without droplets or ice.

Fortin et al. [4] developed a model of coupled heat and mass transfer during ice accretion on an airfoil surface. Olagunju [5] analyzed boundary layer flow and showed that the skin-friction drag decreased and heat transfer increased at lower extensibilities. Cheng [6] examined convection from a horizontal isothermal cylinder of elliptical cross section, in fluids with varying viscosities. The local Nusselt number and skin-friction coefficients were reported as functions of the eccentricity angle, for various values of the viscosity-variation parameter, aspect ratio, and Prandtl number. Dhole et al. [7] developed heat transfer correlations of forced

convection past a sphere in the range of $56 < Re_D < 6200$ and $0.76 < Pr < 6400$. Similar correlations were developed for a horizontal cylinder by Datta et al. [8], including effects of nonuniform slot injection and transverse curvature. Effects of viscous dissipation and varying Prandtl numbers on the skin-friction and heat transfer coefficients were reported.

Past studies indicate that a wide diversity of methods and configurations of forced convection has been studied experimentally. In certain cases, analytical methods have been developed to provide additional insight into forced convection correlations. Turbulent convection from a vertical flat surface was examined by Evans et al. [9]. Predicted temperature and velocity profiles showed good agreement with experimental data. Lachi et al. [10] analyzed heat transfer with fourth-order Karman–Pohlhausen polynomials in a similarity solution. Their study involved a time-dependent heat flux, unlike the steady-state conditions examined in this paper.

Lu and Jiang [11] performed experimental and numerical studies of forced convection along a surface with ribs. Thermocouples inserted into the plate measured local temperatures along the surface. The studies investigated the effects of wall ribs on heat transfer enhancement. Hanjalic [12] reported various limitations of experimental techniques associated with measurements of forced convection, including problems with turbulence and magneto-hydrodynamic heat transfer. Convective heat transfer in micro-electronic assemblies was studied experimentally by Bhowmik et al. [13]. The authors used chromel-alumel thermocouples along a chip centerline to measure temperatures between certain upstream and downstream locations within the channel. The results correlated the Nusselt number variations against the Reynolds number and Grashof number, with respect to the channel hydraulic diameter. Naterer [14,15] correlated transient variations of thermocouple temperature measurements with entropy changes, which led to unique insight regarding convective instabilities within the flowfield. Other experimental studies have used thermistors to determine the local heat transfer coefficients in external flows. For example, Kendoush and Izzat [16] used thermistors to determine the heat transfer coefficients in the wake region of a circular disk in crossflow, between Reynolds numbers of 1.4×10^3 and 5×10^4. Kobus [17] developed an experimental technique to determine convective heat transfer coefficients from thermistor measurements in a circular disk configuration. Self-heating thermistors were used to measure the heat transfer rate and average wall temperature. This brief review of past studies indicates that many past methods have been developed to measure heat transfer coefficients in external flow convection problems.

In this paper, an experimental method will use thermocouples embedded within a hollow airfoil, which is heated internally and cooled externally. Because of approximately 1-D heat conduction within a thin airfoil surface, the temperature difference across the surface leads to a close approximation of the Fourier conduction flux, which balances the convective heat flux in steady-state conditions. Experimental data will then be presented in terms of a nondimensional modified Hilpert correlation for the Nusselt number. Measured results will be illustrated at varying Reynolds numbers, air temperatures, positions along the airfoil surface, and different angles of attack (AOAs).

II. Experimental Apparatus and Procedures

This section describes the experimental setup of forced convection from a NACA 63-421 airfoil in a refrigerated wind tunnel (see Fig. 1). The test section is a square duct, 916 mm in width and 916 mm in height. The wind tunnel is a closed recirculating type that performs cooling immediately downstream of the test section. The wall of the test section is transparent, so observations and photographs can be readily obtained. The test piece is mounted horizontally within the test section. The velocity in the wind tunnel reaches up to 42 m/s at temperatures down to −35°C. The air velocity is adjusted through an electrical control panel by varying the frequency of the motor, which drives the wind-tunnel fan. Further

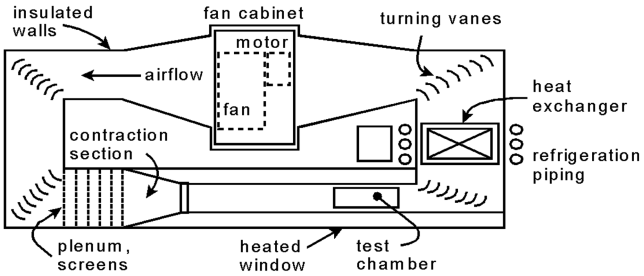

Fig. 1 Top view of wind tunnel.

details regarding the wind-tunnel setup and associated instrumentation were documented previously [18,19].

A 3-D scanner was used to obtain the NACA profile representation of the airfoil. The interior of the airfoil is hollow to reduce its weight. Figure 2 shows the front view and chord of the airfoil. The airfoil chord, span, and thickness are 500, 187.5, and 100 mm, respectively. Three sections of airfoil (each with a 62.5-mm span) were installed side by side to give a total span of 187.5 mm. The airfoil is fabricated with fiberglass and mounted in an aluminum frame inside the test section of the wind tunnel. The thickness of the airfoil fiberglass wall is 3 mm. T-type thermocouples are embedded with the center section of the airfoil surface. The thermocouple junctions are mounted flush with each surface at several positions around the airfoil as shown in Fig. 2. All thermocouple wires are gathered internally within the hollow section of the airfoil.

Electrical heater strips are installed along the inner edges of the airfoil. The dimensions of the heating strips are 40 mm in width and 880 mm in length. The operating voltage of the heating strip is 120 V and the power input is set to 500 W for these experiments. The heater can be adjusted by a variable transformer over a range of voltages between 0 and 120 V. The heater strips are fastened to the inside of the airfoil with double-sided adhesive tape after the thermocouples are installed.

T-type thermocouples are used in a differential connection mode. A direct-reading temperature sensor was used to measure the temperature of the reference junction for cold-junction compensation. The measurement system is controlled by a Labview software program. The experiment uses a total of 25 thermocouples mounted at various locations within the airfoil (see Fig. 2), including 22 thermocouples installed along the inner and outer surfaces of the airfoil. Temperature differences between inner and outer surfaces are measured at 11 different locations.

A thermocouple is inserted in the midplane of the wind tunnel. Figure 3 shows the airfoil at 0 and 15-deg AOAs installed in the wind tunnel. The black center piece is the instrumented airfoil and the lighter side pieces are attached airfoils to remove edge effects as shown in Fig. 3. Through the noninstrumented end pieces, efforts were made to ensure that three-dimensional variations of the temperature and velocity profiles in the z direction (along the shaft in Fig. 3) above the center instrumented piece would be minimized. In this paper, AOAs of 5, 10, 15, 20, and 25 deg are investigated and the results are compared with the 0-deg AOA.

The rate of convective heat transfer from the airfoil is determined by

$$q_{\text{con}} = h(T_o - T_\infty) \tag{1}$$

which can be rearranged as

$$h = \frac{q_{\text{con}}}{T_o - T_\infty} \tag{2}$$

Heater strips below the airfoil surface provide a source of heat input, which is transported through the thin airfoil surface by conduction, then convection to the external airstream. Heat conduction perpendicular to the surface is much larger than lateral heat conduction, due to the high temperature difference across the thin surface. The heaters were installed inside of the airfoil (see Figs. 2 and 3) and the test piece was surrounded by two end pieces.

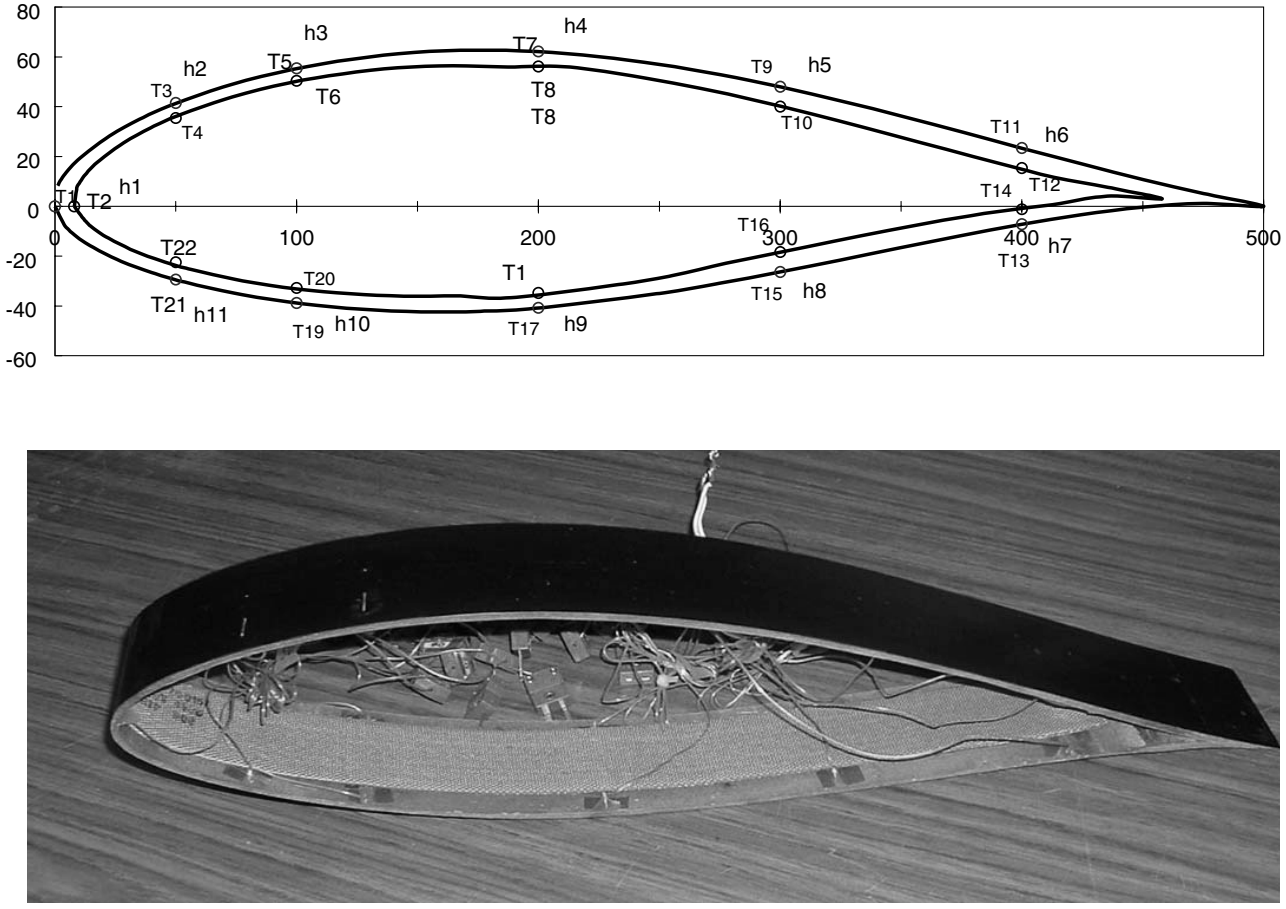

Fig. 2 a) Distribution of measurement points on test airfoil and b) a photograph of the instrumented test airfoil.

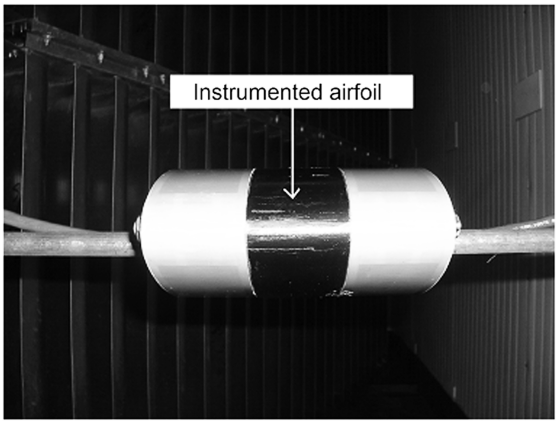

a)

b)

Fig. 3 Instrumented airfoil (middle) mounted in the wind tunnel at a) 0 deg and b) 15 deg AOA.

While the heater was operating, the temperatures along the inner and outer surfaces of the airfoil were measured. Under steady-state conditions, any heat loss internally through the backside of the airfoil remains uniform over time. The heat transfer rate was determined from embedded thermocouple measurements within the wall of the airfoil, rather than electrical power dissipated from the attached heater strips. These thermocouple measurements within the wall yield a Fourier heat flux that closely approximates the supply of heat input to the wall from the heater because of the very thin wall thickness and high temperature difference perpendicular to the wall. From a dimensional analysis, it can be shown that heat conduction perpendicular to the surface is much larger than lateral heat conduction, due to the high temperature difference across the thin surface. The thickness of the airfoil is very thin (3 mm) compared with the chord (500 mm) and span (62.5 mm), so heat transfer is predominantly one dimensional across the wall of the airfoil.

The perpendicular Fourier heat flux balances the rate of convective heat transfer to the surrounding airstream, thereby leading to the following result:

$$q_{\text{con}} = q_{\text{cd}} = \frac{k(T_i - T_o)}{\delta} \tag{3}$$

Substituting Eq. (2) into Eq. (3), the resulting heat transfer coefficient can be expressed in the following manner:

$$h = \frac{k(T_i - T_o)}{\delta(T_o - T_\infty)} \tag{4}$$

The average heat transfer coefficient was obtained from spatial averaging around the airfoil with the following result:

$$\bar{h} = \frac{1}{s}\int_s h\,\mathrm{d}x = \frac{1}{s}\sum_i^{11} h_i \Delta s_i \tag{5}$$

Then, the average Nusselt number becomes

$$\overline{Nu} = \frac{\bar{h}c}{k_{\text{air}}} \tag{6}$$

In the following section, results of both local and average Nusselt numbers will be examined. The experimental uncertainty of the measured Nusselt number depends on the uncertainty of the local heat transfer coefficient, airfoil chord, thermal conductivity, and geometrical factors. The local heat transfer coefficient depends on the temperature difference between the surface and the freestream, as well as the net convective heat loss for each test case. In the next section, a detailed analysis of measurement uncertainties is presented.

III. Analysis of Measurement Uncertainties

The method of Kline and McClintock [20] is used to determine the measurement uncertainties in the heat transfer experiments. In the experiments, the parameters T_o, T_i, T_∞, and δ were measured. The total uncertainty U_h depends on P_h and B_h, which are the precision and bias limits for each variable and parameter contribution to the total uncertainty, that is,

$$U_h = \sqrt{P_h^2 + B_h^2} \tag{7}$$

The precision contribution can be calculated with the following propagation equation, which extends the method of Kline and McClintock [20] to the current problem parameters as follows:

$$P_h^2 = \left(\frac{\partial h}{\partial T_i}\right)^2 P_{Ti}^2 + \left(\frac{\partial h}{\partial T_o}\right)^2 P_{To}^2 + \left(\frac{\partial h}{\partial T_\infty}\right)^2 P_{T\infty}^2 + \left(\frac{\partial h}{\partial \delta}\right)^2 P_\delta^2 + \left(\frac{\partial h}{\partial k}\right)^2 P_k^2 \tag{8}$$

Using Eq. (4) to evaluate the derivatives and defining $\Delta T_1 = T_i - T_o$ and $\Delta T_2 = T_o - T_\infty$, it can be shown that Eq. (8) leads to

$$\left(\frac{P_h}{h}\right)^2 = \left(\frac{P_{Ti}}{\Delta T_1}\right)^2 + \left(\frac{P_{To}}{\Delta T_2}\right)^2 + \left(\frac{P_{T\infty}}{\Delta T_2}\right)^2 + \left(\frac{P_\delta}{\delta}\right)^2 + \left(\frac{P_k}{k}\right)^2 \tag{9}$$

Using a similar procedure, it can be shown that the following result is obtained for the bias contribution:

$$\left(\frac{B_h}{h}\right)^2 = \frac{B_{Ti}^2}{\Delta T_1^2} + \left(\frac{1}{\Delta T_1} + \frac{1}{\Delta T_2}\right)^2 B_{To}^2 - 2\left(\frac{1}{\Delta T_1^2} + \frac{1}{\Delta T_1 \Delta T_2}\right) B'_{To} B'_{Ti} + \frac{2}{\Delta T_1 \Delta T_2} B'_{T\infty} B'_{Ti} - 2\left(\frac{1}{\Delta T_2^2} + \frac{1}{\Delta T_1 \Delta T_2}\right) B'_{To} B'_{T\infty} + \frac{B_{T\infty}^2}{\Delta T_2^2} + \frac{B_k^2}{k^2} + \frac{B_\delta^2}{\delta^2} \tag{10}$$

where B'_{Ti}, B'_{To}, and $B'_{T\infty}$ are the portions of B_{Ti}, B_{To}, and $B_{T\infty}$, respectively, which arise from an identical error source, so they are assumed to be perfectly correlated.

The bias contribution to the uncertainty becomes

$$\left(\frac{B_h}{h}\right)^2 = \frac{B_k^2}{k^2} + \frac{B_\delta^2}{\delta^2} \tag{11}$$

Then, the total uncertainty of the heat transfer coefficient becomes

$$\frac{U_h}{h} = \sqrt{\left(\frac{P_h}{h}\right)^2 + \left(\frac{B_h}{h}\right)^2} \tag{12}$$

For the current experiments, $P_{Ti} = P_{To} = P_{T\infty} = 0.64$ K, $\Delta T_1 = 10.25$ K, $\Delta T_2 = 42.42$ K, $P_\delta = 0.095$ mm, $\delta = 2.999$ mm, and $B_\delta = 0.005$ mm. It was assumed that $P_k/k = 0$ and $B_k/k = 0$. Using these parameters, the uncertainty of the heat transfer coefficient becomes $U_h/h = 7.32\%$.

The Nusselt number is $Nu = h_c/k$, so its total uncertainty can be expressed in the following manner:

$$\frac{U_{\overline{\text{Nu}}}}{\overline{Nu}} = \sqrt{\left(\frac{P_{\overline{\text{Nu}}}}{\overline{Nu}}\right)^2 + \left(\frac{B_{\overline{\text{Nu}}}}{\overline{Nu}}\right)^2} = \sqrt{\left(\frac{U_h}{h}\right)^2 + \left(\frac{B_c}{c}\right)^2 + \left(\frac{B_k}{k}\right)^2} = 7.34\% \tag{13}$$

It was determined that the measurement uncertainty of the average freestream velocity is $U_u/u = 0.397\%$. Also, the uncertainties of the tabulated density of air and manometer fluid for the pitot tube measurements of velocity are $U_{\rho 1}/\rho_1 = U_{\rho \text{air}}/\rho_{\text{air}} = 0.5\%$. As a result, the uncertainty of the measured Reynolds number is 0.818%, based on the uncertainty of velocity, density of air, viscosity, and bias of the chord length.

This measurement uncertainty of the Reynolds number indirectly affects the uncertainty of the Nusselt number, through the heat transfer coefficient, which depends on the air velocity and other parameters. Using the above procedure, it was calculated that the measurement uncertainty of the Nusselt number is 7.34%. In the next section, measured data from the experimental procedure will be presented and discussed.

IV. Results and Discussion

Transition to turbulence of a boundary layer over a flat plate occurs at local Reynolds numbers of about $Re_x \geq 5 \times 10^5$. The transition number for a cylinder in crossflow occurs at approximately $Re_D = 2 \times 10^5$. In view of these similarities, experimental correlations will be investigated with the following functional form of the Nusselt number, which is equivalent to the Hilpert correlation for a cylinder in crossflow (reported by Incropera and DeWitt [21]),

$$\overline{Nu} = cRe^m Pr^{1/3} \tag{14}$$

Experimental studies have shown the AOA substantially affects the heat transfer coefficient. Figure 4 shows the measured Nusselt numbers Nu_x at different positions and Reynolds numbers. The curve with AOA = 0 shows that the Nusselt number decreases after the stagnation point, due to the thickening boundary layer along the top and bottom surfaces. It falls to the lowest point at the position of $0.2c$ along the chord of the airfoil, after which it increases. Although both surfaces of the airfoil have the same trends near the leading edge of the airfoil, the lowest value of Nu_x occurs along the bottom surface. It would have the same local Nusselt number, if the airfoil was symmetric in shape and orientation with respect to the freestream, but nonsymmetry leads to different Nusselt number results on each side of the stagnation point. The thickness of the laminar boundary layer increases when x increases from the leading edge to the trailing edge. At certain points along each surface, transition to turbulence occurs within the boundary layer. In the laminar region, the heat transfer coefficient decreases when the thickness of the boundary layer increases. The heat transfer coefficient then increases when the boundary layer becomes turbulent.

In Fig. 4a, it can be observed how the Nusselt number changes with AOA, for the case of a low Reynolds number. At the stagnation point, the Nusselt number remains nearly uniform at different values of AOA. However, it can change significantly with AOA along the chord of the airfoil. The Nusselt number decreases significantly at $\pm 0.1c$, $-0.4c$, and $0.6c$, and it increases at $-0.2c$, -0.6c, and $0.4c$. Figure 4b shows results of the Nusselt number for cases of high Reynolds numbers. At angles of attack of 5 and 10 deg, the local Nusselt number at the stagnation point is lower than the case for 0 deg. Also, values of the Nusselt number at $-0.4c$ and $+0.6c$ are lower than an AOA of zero at those points. In contrast, the values of the Nusselt number at $-0.1c$, $-0.2c$, and $-0.6c$ are higher than the AOA of zero at the same points. As the AOA increases, the changes

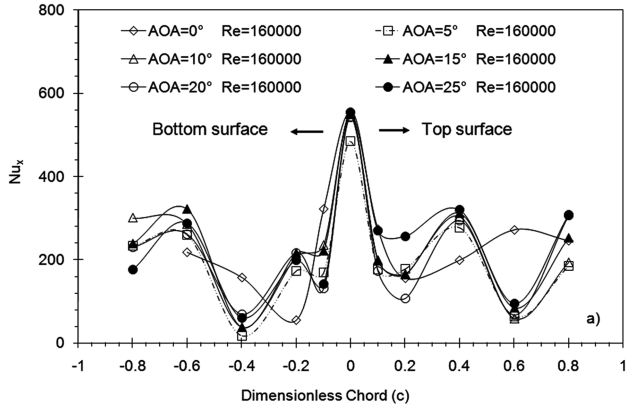

a)

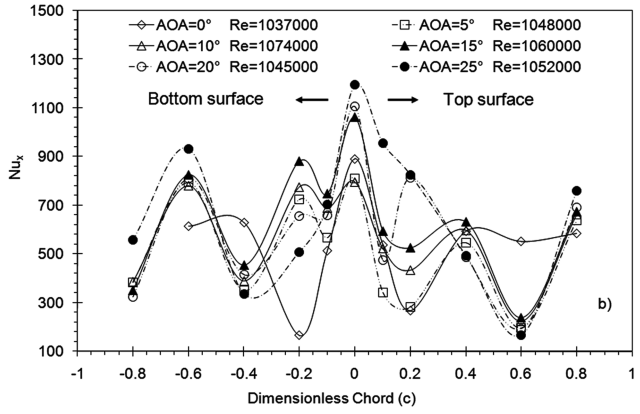

b)

Fig. 4 Local Nusselt number distribution along the dimensionless chord and a) low Re_c and b) high Re_c.

of local Nusselt number with AOA become more pronounced at higher Reynolds numbers. The Nusselt number at the stagnation point is higher than the value of the Nusselt number at the stagnation point when the angle of attack is 0 deg. Also, only two points of the local Nusselt number along the airfoil, $-0.4c$ and $+0.6c$, have lower values than the Nusselt number at 0 deg for the same points. The values of Nu_x for the other points along the airfoil are larger than the local Nusselt number at the same points for 0 deg. The average Nusselt number is expected to have similar distinct trends at high Reynolds numbers. Experiments were initially conducted for zero AOA between dimensionless cord positions of 0.8 and -0.6, while separate studies were conducted afterward with other thermocouple measurements.

Along the top surface after chord positions of 0.2 and 0.6, as well as chord positions -0.1 and -0.4 along the lower surface, the local Nusselt number rises abruptly. These trends may be attributed to transition from laminar to turbulent boundary flow (near the leading edge), as well as flow separation (near the trailing edge). The location of flow separation varies with the angle of attack. The movement of the point of separation depends on the magnitude of the adverse pressure gradient, angle of attack, and Reynolds number [22]. When the Reynolds number increases, the separation point moves toward the leading edge. Higher turbulence over the airfoil will enhance the heat transfer at higher Reynolds number. A recirculation region develops and moves toward the leading edge, when the angle of attack increases. A higher Reynolds number will lead to a circulation region at the smaller angle of attack, when the center of recirculation moves forward to the leading edge. These mechanisms explain various trends that were observed for heat transfer results in Figs. 4a and 4b along the airfoil at different AOA and Reynolds numbers.

The following form of correlation has been used previously by Van Fossen et al. [2] for an iced airfoil:

$$\overline{Nu} = ARe^{B} \tag{15}$$

where A and B are coefficients that depend on flow conditions. This functional form is similar to Nusselt number correlations obtained previously by Wang et al. [23] for convective heat transfer from an airfoil at 0-deg AOA and associated formula corrections. The relationships between Reynolds and Nusselt number coefficients [c and m in Eq. (14)] were determined based on a least-squares curve fit of measured data by Wang et al. [23]. The following correlations were obtained for convective heat transfer from an uniced airfoil:

$$\overline{Nu} = 0.0943Re_c^{0.636}Pr^{1/3} \qquad (\text{for } Re_c > 5 \times 10^5) \tag{16}$$

$$\overline{Nu} = 2.482Re_c^{0.389}Pr^{1/3} \qquad (\text{for } Re_c \le 5 \times 10^5) \tag{17}$$

For different AOAs, a similar functional form will be used, but modified for varying angles of attack. A modified heat transfer correlation is developed according to the following functions:

$$\overline{Nu} = 0.0943(C_1 + D_1\alpha)Re_c^{0.636}Pr^{1/3} \tag{18}$$

$$\overline{Nu} = 2.482(C_1 + D_2\alpha)Re_c^{0.389}Pr^{1/3} \tag{19}$$

where α, C_1, D_1, and D_2 refer to the AOA and coefficients used as correction factors in the correlations developed for the limiting case of zero angle of attack. The normalized chord of the airfoil (c) and dynamic center (c_m) are used to define the first coefficient, $C_1 = 1 - c_m/c = 1 - 0.25/1 = 0.75$ for nonzero angles of attack, but $C_1 = 1$ at zero AOA. In this way, Eqs. (18) and (19) reduce to Eqs. (16) and (17), respectively, at zero AOA. The remaining coefficients are found from a unit angle and exchange factor from 1 deg to the maximum arclength: $D_1 = \pi/180 = 0.017$ and $D_2 = C_1 \times D_1 = 0.013$. These coefficients aim to provide a functional expression that accounts for movement of the point of separation along the airfoil surface, due to varying angles of attack. By including the AOA correction factor based on this movement, the expected Nusselt number trends for varying angles of attack can be established in a modified Hilpert correlation of convective heat transfer.

The coefficient D_2 must be modified differently by D_1 and C_1, for cases of lower turbulence when movement of the transition point changes at low Reynolds numbers. Using these resulting factors in Eqs. (18) and (19), the following correlations are obtained for the Nusselt number in low and high Reynolds number cases, respectively:

$$\overline{Nu} = 0.0943(0.75 + 0.017\alpha)Re_c^{0.636}Pr^{1/3} \quad (\text{for } Re_c > 5 \times 10^5) \tag{20}$$

$$\overline{Nu} = 2.482(0.75 + 0.013\alpha)Re_c^{0.389}Pr^{1/3} \quad (\text{for } Re_c \le 5 \times 10^5) \tag{21}$$

Figure 5 shows better agreement between measured data and predictions at AOA $= 10$ deg, when the above correction factors are applied to the Nusselt number correlation. Measured data at varying temperatures (different Prandtl numbers) are illustrated in Fig. 5. Without the above correction factors, the zero AOA correlation would overpredict the measured data across the range of Reynolds numbers. For the results in Fig. 5, the curve regression coefficient is $R^2 = 0.955$. Unlike a past similar study by Wang et al. [24] that examines the convective transfer with impinging droplets on a NACA airfoil, the current results involve airflow only (without droplets). The current formulation improves upon earlier correlations in terms of the dependence on varying angles of attack, without droplets.

Figure 6 shows additional results for other angles of attack: 5, 10, 15, 20, and 25 deg at higher Reynolds numbers. In each case, the correction factors for Nusselt number correlations have yielded good agreement between the predicted and measured data. In Fig. 6, the Nusselt number decreases when the angle of attack rises from 0 to

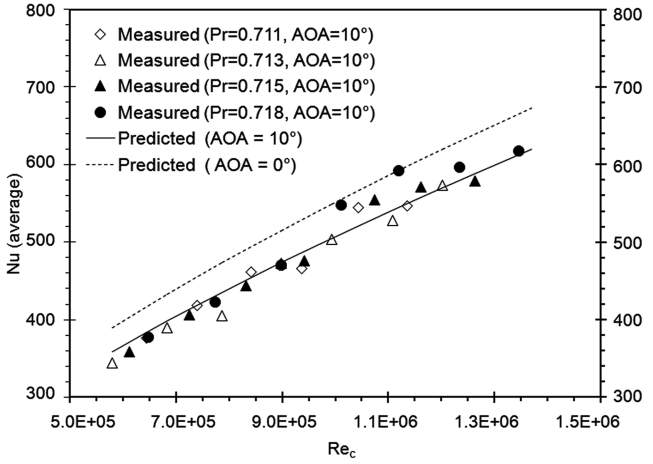

Fig. 5 Comparison of measured data at 10 deg and Nusselt number correlations at 0 and 10 deg AOA.

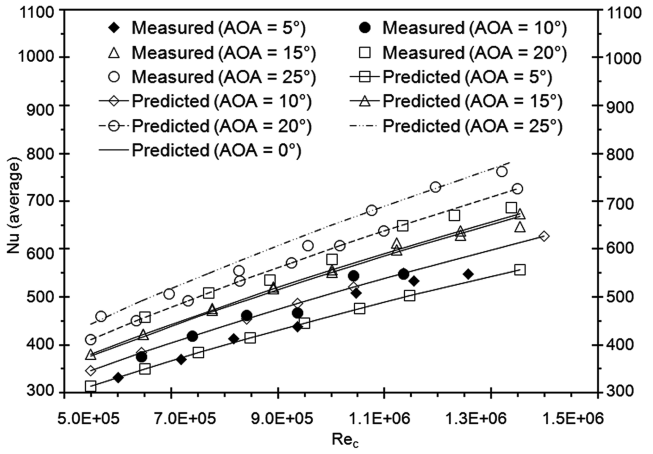

Fig. 6 Measured data and Nusselt number correlation at various AOAs (high Re_c).

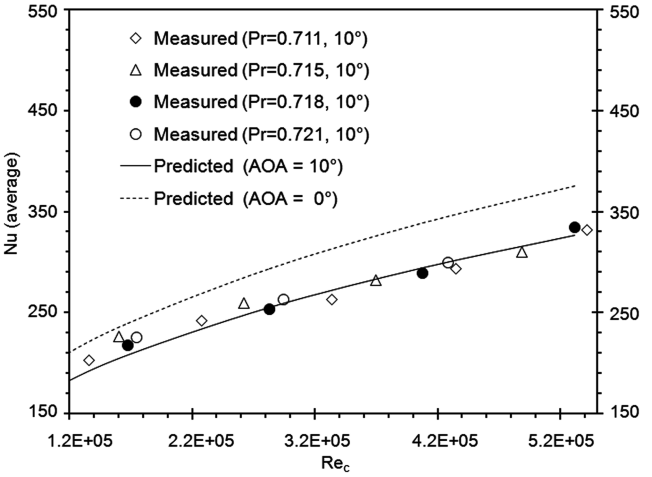

Fig. 7 Measured data and Nusselt number correlation at 10 deg AOA (low Re_c).

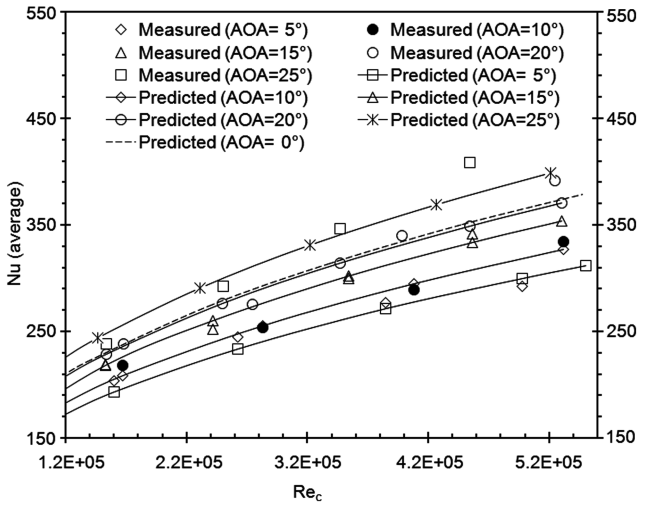

Fig. 8 Measured data and Nusselt number correlation at varying AOAs from 5 to 25 deg (low Re_c).

5 deg, but then it increases thereafter at higher AOAs. At low angles of attack, the boundary layer thickness increases along the trailing edge, thereby reducing the near-wall temperature gradient and heat transfer coefficient. However, at higher AOA, the separation point moves upstream, induces turbulence, and enhances heat exchange, thereby explaining the larger Nusselt number at higher angles of attack.

Additional results at lower Reynolds numbers show that close agreement is also achieved between measured and predicted data at 10 deg (Fig. 7) and higher angles of attack (Fig. 8). As observed previously for higher Reynolds numbers, the Nusselt number increases at higher angles of attack. The predicted trends of 0 and 10 deg AOA in Figs. 5 and 7 refer to corrected correlations, not trends at different angles of attack from the same correlation. In other words, a zero AOA curve is shown to initially deviate from the measured data, so a corrected correlation at 10 deg AOA is used instead. The corrected correlation is different than the correlation used previously for the zero AOA case. The purpose is to demonstrate that the AOA correction can be used to predict the measured trends associated with varying angles of attack, rather than sensitivity of the Nusselt number to varying AOA. In conclusion, the results in this section indicate that a standard Hilpert form of convection correlation can be used to predict heat transfer from a NACA airfoil at varying angles of attack. A correction factor on a standard Hilpert correlation has yielded close agreement with measured data of the Nusselt number.

V. Conclusions

This paper has developed a modified Hilpert correlation of forced convection heat transfer from a NACA airfoil at different angles of attack. An experimental method was developed with thermocouples embedded at different locations along the surface of the airfoil. Under steady-state conditions, heat conduction through the airfoil was balanced against heat transfer by convection to the airstream. It was determined that experimental data could be collapsed onto a normalized correlation of $Nu/Pr^{1/3}$ at varying Prandtl numbers. Representative coefficients of the modified Hilpert correlation were reported. It was observed that the average Nusselt number varied at different angles of attack, due to movement of the transition point, recirculation zone, and transition to turbulence. The correction factors and modified correlations have provided useful new tools for heat transfer from airfoils at varying angles of attack.

Acknowledgments

Financial support of this research from the Natural Sciences and Engineering Research Council of Canada and the Canada Foundation for Innovation are gratefully acknowledged.

References

[1] Naterer, G. F., *Heat Transfer in Single and Multiphase Systems*, CRC Press, Boca Raton, FL, 2003.

[2] Van Fossen, G. J., Simoneau, R. J., Olsen, W. A., and Shaw, R. J., "Heat Transfer Distributions Around Nominal Ice Accretion in the LEWIS Icing Research Tunnel," AIAA Paper 84-0017, 1984.

[3] Henry, R. C., Guffond, D., Bouveret, A., and Gardette, G., "Heat Transfer Coefficient Measurement on Iced Airfoil in a Small Icing Wind Tunnel," AIAA Paper 99-0372, 1999.

[4] Fortin, G., Laforte, J. L., and Ilinca, A., "Heat and Mass Transfer During Ice Accretion on Aircraft Wings with an Improved Roughness Model," *International Journal of Thermal Sciences*, Vol. 45, No. 6, 2006, pp. 595–606. doi:10.1016/j.ijthermalsci.2005.07.006

[5] Olagunju, D. O., "A Self-Similar Solution for Forced Convection Boundary Layer Flow of a FENE-P Fluid," *Applied Mathematics Letters*, Vol. 19, No. 5, 2006, pp. 432–436. doi:10.1016/j.aml.2005.05.015

[6] Cheng, C. Y., "The Effect of Temperature-Dependent Viscosity on the Natural Convection Heat Transfer from a Horizontal Isothermal Cylinder of Elliptic Cross Section," *International Communications in Heat and Mass Transfer*, Vol. 33, No. 8, 2006, pp. 1021–1028. doi:10.1016/j.icheatmasstransfer.2006.02.019

[7] Dhole, S. D., Chabra, R. P., and Eswaran, V., "A Numerical Study on the Forced Convection Heat Transfer from an Isothermal and Isoflux Sphere in the Steady Symmetric Flow Regime," *International Journal of Heat and Mass Transfer*, Vol. 49, No. 5, 2006, pp. 984–994. doi:10.1016/j.ijheatmasstransfer.2005.09.010

[8] Datta, P., Anilkumar, D., Roy, S., and Mahanti, N. C., "Effect of Non-Uniform Slot Injection (Suction) on a Forced Flow over a Slender Cylinder," *International Journal of Heat and Mass Transfer*, Vol. 50, No. 15, 2007, pp. 3190–3194. doi:10.1016/j.ijheatmasstransfer.2007.01.006

[9] Evans, G., Greif, R., Siebers, D., and Tieszen, S., "Turbulent Mixed Convection from a Large, High Temperature, Vertical Flat Surface," *International Journal of Heat and Fluid Flow*, Vol. 26, No. 1, 2005, pp. 1–11. doi:10.1016/j.ijheatfluidflow.2004.07.001

[10] Lachi, M., Rebay, M., Mladin, E. C., and Padet, J., "Alternative Models for Transient Convection Heat Transfer in External Flows over a Plate Exposed to a Variable Heat Flux," *International Journal of Thermal Sciences*, Vol. 43, No. 8, 2004, pp. 809–816. doi:10.1016/j.ijthermalsci.2004.02.021

[11] Lu, B., and Jiang, P. X., "Experimental and Numerical Investigation of Convection Heat Transfer in a Rectangular Channel with Angled Ribs," *Experimental Thermal and Fluid Science*, Vol. 30, No. 6, 2006, pp. 513–521. doi:10.1016/j.expthermflusci.2005.09.007

[12] Hanjalic, K., "Synergy of Experiments and Computer Simulations in Research of Turbulent Convection," *International Journal of Heat and Fluid Flow*, Vol. 26, No. 6, 2005, pp. 828–842. doi:10.1016/j.ijheatfluidflow.2005.10.007

[13] Bhowmik, H., Tso, C. P., Tou, K. W., and Tan, F. L., "Convection Heat Transfer from Discrete Heat Sources in a Liquid Cooled Rectangular Channel," *Applied Thermal Engineering*, Vol. 25, No. 16, 2005, pp. 2532–2542. doi:10.1016/j.applthermaleng.2004.11.022

[14] Naterer, G. F., "Establishing Heat—Entropy Analogies for Interface Tracking in Phase Change Heat Transfer with Fluid Flow," *International Journal of Heat and Mass Transfer*, Vol. 44, No. 15, 2001, pp. 2903–2916. doi:10.1016/S0017-9310(00)00334-3

[15] Naterer, G. F., "Applying Heat—Entropy Analogies with Experimental Study of Interface Tracking in Phase Change Heat Transfer," *International Journal of Heat and Mass Transfer*, Vol. 44, No. 15, 2001, pp. 2917–2932. doi:10.1016/S0017-9310(00)00296-9

[16] Kendoush, A. A., and Izzat, A. W., "Experiments of Fluid Flow and Heat Convection in the Wake of a Disk Facing a Uniform Stream," *International Journal of Thermal Sciences*, Vol. 44, No. 9, 2005, pp. 894–902. doi:10.1016/j.ijthermalsci.2005.02.005

[17] Kobus, C. J., "Utilizing Disk Thermistors to Indirectly Measure Convective Heat Transfer Coefficients for Forced, Natural and Combined (Mixed) Convection," *Experimental Thermal and Fluid Science*, Vol. 29, No. 6, 2005, pp. 659–669. doi:10.1016/j.expthermflusci.2004.10.001

[18] Naterer, G. F., Popplewell, N., Barrett, W., Anderson, J., Faraci, E., McCartney, D., and Lehmann, W., "Experimental Facility for New Hybrid Ice/Spray Flow Tunnel with Laser Based Droplet Measurement," AIAA Paper 2002-2867, June 2002.

[19] Wang, X., Naterer, G. F., and Bibeau, E., "Experimental Study of 3-D Blades and Wind Turbines Under Icing Conditions," *International Green Energy Conference*, University of Ontario Institute of Technology, Oshawa, Ontario, Canada, 25–29 June 2006.

[20] Kline, S. J., and McClintock, F. A., "Describing Uncertainties in Single-Sample Experiments," *Mechanical Engineering*, Vol. 75, 1953, pp. 3–8.

[21] Incropera, F. P., and DeWitt, D. P., *Fundamentals of Heat and Mass Transfer*, 4th ed., Wiley, New York, 1996, Chap. 7.

[22] Montelpare, S., and Ricci, R., "A Thermographic Method to Evaluate the Local Boundary Layer Separation Phenomena on Aerodynamic Bodies Operating at Low Reynolds Number," *International Journal of Thermal Sciences*, Vol. 43, No. 3, 2004, pp. 315–329. doi:10.1016/j.ijthermalsci.2003.07.006

[23] Wang, X., Bibeau, E., and Naterer, G. F., "Experimental Correlation of Forced Convection Heat Transfer from a NACA Airfoil," *Experimental Thermal and Fluid Science*, Vol. 31, No. 8, 2007, pp. 1073–1082. doi:10.1016/j.expthermflusci.2006.11.008

[24] Wang, X., Naterer, G. F., and Bibeau, E., "Multiphase Nusselt Correlation for the Impinging Droplet Heat Flux from a NACA Airfoil," *Journal of Thermophysics and Heat Transfer*, Vol. 22, No. 2, 2008, pp. 219–226. doi:10.2514/1.32401